Contents lists available at ScienceDirect

Bioactive Materials

A bioactive glass functional hydrogel enhances bone augmentation via synergistic angiogenesis, self-swelling and osteogenesis

Fujian Zhao [a,1], Zhen Yang [b,c,1], Huacui Xiong [a], Yang Yan [b,c], Xiaofeng Chen [b,c,*], Longquan Shao [a,d,**]

[a] Stomatological Hospital, Southern Medical University, Guangzhou, 510280, China
[b] Department of Biomedical Engineering, School of Materials Science and Engineering, South China University of Technology, Guangzhou, 510641, China
[c] National Engineering Research Center for Tissue Restoration and Reconstruction, South China University of Technology, Guangzhou, 510006, China
[d] Guangdong Provincial Key Laboratory of Construction and Detection in Tissue Engineering, Guangzhou, 510515, China

A B S T R A C T

Bone augmentation materials usually cannot provide enough new bone for dental implants due to the material degradation and mucosal pressure. The use of hydrogels with self-swelling properties may provide a higher bone augmentation, although swelling is generally considered to be a disadvantage in tissue engineering. Herein, a double-crosslinked gelatin-hyaluronic acid hydrogels (GH) with self-swelling properties were utilized. Meanwhile, niobium doped bioactive glasses (NbBG) was dispersed in the hydrogel network to prepare the GH-NbBG hydrogel. The composite hydrogel exhibited excellent biocompatibility and the addition of NbBG significantly improved the mechanical properties of the hydrogel. *In vivo* results found that GH-NbBG synergistically promoted angiogenesis and increased bone augmentation by self-swelling at the early stage of implantation. In addition, at the late stage after implantation, GH-NbBG significantly promoted new bone formation by activating RUNX2/Bglap signaling pathway. Therefore, this study reverses the self-swelling disadvantage of hydrogels into advantage and provides novel ideas for the application of hydrogels in bone augmentation.

1. Introduction

With the loss of natural teeth, the alveolar ridge undergoes severe atrophy, which cannot provide enough bone for dental implants. Autologous bone grafting is the gold standard for bone augmentation, but it is difficult to popularize in clinic due to the high surgical trauma [1]. Replacing autologous bone grafts with biomaterials can avoid these deficiencies [2]. However, due to mucosal pressure and material degradation, the final bone augmentation height is lower than the original material implantation, which still cannot provide enough bone for the dental implant.

The use of materials with swelling properties may provide greater bone augmentation than the material at the original height. For example, hydrogel is a kind of self-swelling polymer material after absorbing water [3]. Due to their similar composition to the extracellular matrix, hydrogels have been widely used in tissue engineering, including in bioprinting, drug release and tissue repair [4,5]. In most applications of hydrogels, swelling is generally considered a disadvantage, which will weaken its mechanical properties, oppress the surrounding tissue and impedes normal metabolism. Therefore, many methods have been used to inhibit the self-swelling of hydrogels [6–8]. However, at the position of alveolar ridge atrophy, the hydrogel is expected to swell as much as possible to achieve more bone augmentation. Therefore, this "disadvantage" can be turned into an "advantage" in the application of bone augmentation.

The swelling of hydrogel without limits will lead to the decrease of mechanical properties and collapse. To solve this problem, appropriate crosslinking methods are necessary, which will achieve accurate control of hydrogel self-swelling [9]. The addition of inorganic components into hydrogel system can also improve the mechanical properties, especially

some micro-nano particles [10–12]. For example, the addition of micro-nano bioactive glasses (MNBG) into hydrogels can improve compressive strength [13]. MNBG is a kind of microsphere with uniform particle size and excellent biological activity [14]. The osteogenesis capacity of MNBG has been widely recognized due to its rapid ion dissolution property, which has been widely used in dentistry and bone repair [15,16]. However, the use of MNBG for bone augmentation is rarely reported. Our previous works have found that MNBG can directly form new bone outside the cortical bone to achieve bone augmentation [17]. However, the final bone augmentation height is significantly reduced due to the degradation of the MNBG. Therefore, the combination of MNBG with hydrogels is expected to achieve a greater height of bone augmentation by using the self-swelling properties of hydrogels.

When a hydrogel is implanted into the bone augmentation position, local ischemia will occur due to excessive mucosal tension [18]. Especially with the swelling of hydrogel, ischemia will be aggravated. Therefore, it is urgent to form a large number of blood vessels at the early stage of hydrogel implantation. However, only using MNBG to promote angiogenesis is obviously insufficient [19–21]. Doping metal ions with therapeutic effects is a simple method to endow MNBG with specific functions including osteogenesis and angiogenesis [22,23]. For example, niobium (Nb) has been reported to be incorporated into bioactive glasses (BG) for bone repair [24,25]. However, experimental evidence on whether Nb doped bioactive glass (NbBG) could promote early angiogenesis has rarely been reported. In addition to the early rapid vascularization, osteogenesis at the later stage of implantation is also critical for bone augmentation. NbBG has been reported to promote osteogenesis in bone defect areas [26,27]. However, whether NbBG has the same osteogenic effect on bone augmentation position has not been reported. In addition, the mechanism of NbBG promoting osteogenesis is unclear.

In the ancient Chinese myth of "*Pan Gu epoch*", Pan Gu (the creator of the universe in Chinese mythology) separated the merged sky from the earth. Then, he gradually expanded the distance between the sky and the earth by stretching his body, and finally his body became mountains and rivers when he was exhausted and died (Fig. 1A). Inspired by the Chinese ancient myth of "*Pan Gu epoch*", we prepared a double crosslinked gelatin-hyaluronic acid hydrogels (GH) by oxidized hyaluronic acid (HA-CHO) and tyramine modified gelatin (GA-tyramine). The NbBG was added to the hydrogel to fabricate a kind of inorganic strengthened GH-NbBG hydrogels which was likened to "Pan Gu" (Fig. 1C). After the GH-NbBG hydrogel was implanted into the bone augmentation area, the self-swelling property was beneficial for achieving the elevation of the alveolar ridge, and NbBG promoted angiogenesis during the expansion process. Finally, the hydrogel degrades and forms new bone, which is successfully implanted into the dental implant (Fig. 1B). The mechanical property, biocompatibility, angiogenesis and osteogenesis of the GH-NbBG were investigated both *in vitro* and *in vivo*. In addition, the osteogenesis mechanism of GH-NbBG was further studied.

2. Materials and methods

2.1. Synthesis and characterization of NbBG

The synthesis and characterizations of monodispersed BG and NbBG microspheres was performed according to our previous report [17]. The molar composition of BG and NbBG were $60SiO_236CaO4P_2O_5$ and $60SiO_226CaO10Nb_2O_54P_2O_5$, respectively. In brief, a given amount of dodecylamine (DDA) was dissolved in 25 mL deionized water and 80 mL Ethanol. Then, 16 mL tetraethyl orthosilicate (TEOS) were added to the above solutions and stirred for 1 h. After that, triethylphosphate (TEP) and calcium nitrate tetrahydrate (CN) or $NbCl_5$ were added in order in the proportions at 30 min intervals while magnetically stirring at 40 °C. The resulted solution was vigorously stirred together for another 3 h,
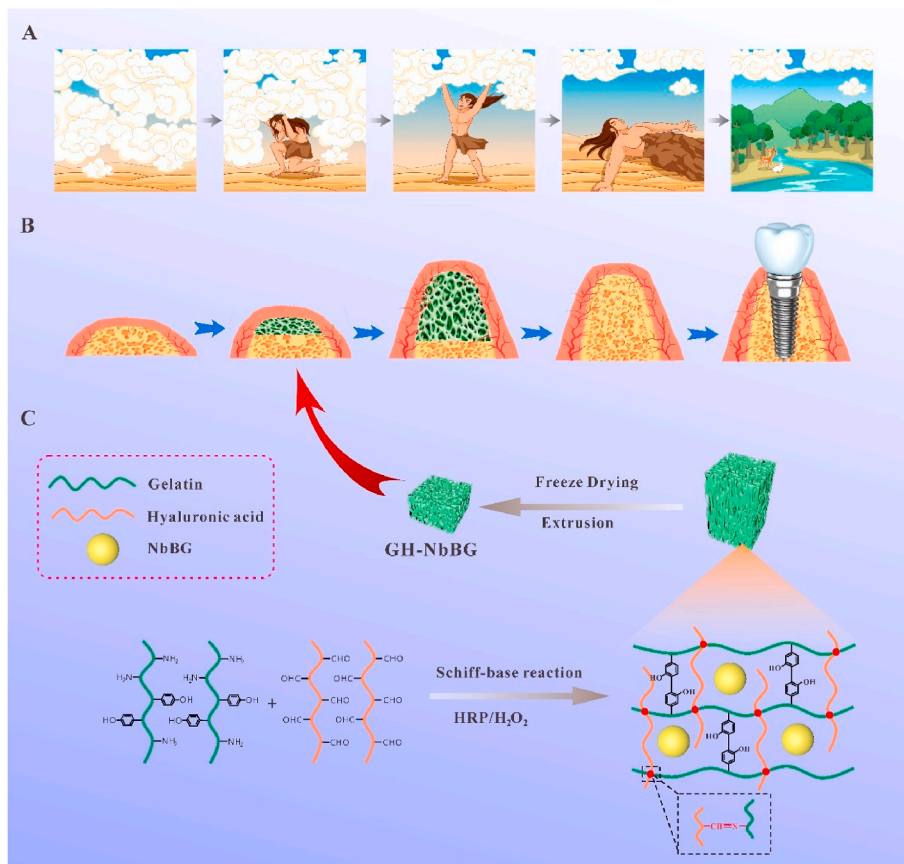

Fig. 1. Schematic illustration. (A) The myth of "*Pan Gu epoch*": sky and earth were combined and inseparable at first. Then, Pan Gu separated the merged sky from the earth. Subsequently, he gradually increased the distance between the sky and the earth, through extension of his body, and finally his body became mountains and rivers after death; (B) GH-NbBG is used for bone augmentation which is corresponds to "*Pan Gu epoch*": After implanted into the bone augmentation area, the GH-NbBG hydrogels synergistically promoted angiogenesis and increased bone augmentation by self-swelling. Finally, the hydrogels degrades and forms new bone which is successfully implanted into the dental implant; (C) Preparation of GH-NbBG hydrogels by NbBG added in Schiff base reaction and HRP/H_2O_2 enzyme cross linking reaction.

and the white precipitates were collected by filtration and dried at 60 °C for 24 h. BG and NbBG were obtained after removing templates and organic components by calcifying under air atmosphere at 650 °C for 3 h. The morphology and structure of the microspheres were characterized by scanning electron microscopy (SEM, Merlin Carl Zeiss Jena, Germany), energy dispersive spectroscopy (EDS). The chemical composition and valence state of the microspheres were characterized by Fourier Transform Infrared Spectrometry (FTIR, VERTEX 33 Bruker, Germany), X-ray photoelectron spectroscopy (XPS, Thermo Scientific K-Alpha, USA) and X-ray diffractometer (XRD, Bruker D8, Netherlands).

2.2. Synthesis and characterization of HA-CHO and GA-tyramine

For the preparation of aldehyde modified hyaluronic acid (HA-CHO), 1.0 g HA were dissolved in 200 mL deionized water with stirring to form a homogeneous solution at room temperature. Then 1.13 g $NaIO_4$ were dissolved in 15 mL deionized water and added dropwise to the HA solution, the mixed solution was vigorously stirred for another 2 h. At last, 1 mL ethylene glycol was added into the solution and stirred for another 1 h. Thereafter, the sample was dialyzed against distilled water for 3 days (Mw cut-off, 8k-14k), the final product was obtained by freeze-drying.

To prepare the tyramine modified gelatin (GA-tyramine), 10 g GA was added to 500 mL MES buffer (50 mM, pH = 5.0), the solution was heated to 50 °C with stirring until the gelatin had completely dissolved, and then cooled the solution to room temperature. Next, 5 g tyramine hydrochloride, 0.74 g EDC and 0.22 g NHS were added to GA solution respectively, the mixture was allowed to react at 25 °C for 24 h. The unreacted tyramine hydrochloride was dialyzed against deionized water for 3 days (Mw cut-off, 3.5k) and the final product was obtained by freeze-drying. The qualitative modifications of HA and GA were confirmed by ^1H nuclear magnetic resonance (^{1}HNMR, Bruker, Germany).

2.3. Synthesis and characterization of GH-NbBG hydrogels

750 mg GA-tyramine was dissolved in 2.5 mL deionized water containing 50 mg NbBG at 60 °C. Meanwhile, 250 mg HA-CHO was dissolved in 2.5 mL deionized water. These two solutions were mixed rapidly at 800 rpm for 5 min containing 50 unit/mL peroxidase from horseradish (HRP) and then injected into the mold. After 1 h, GH-NbBG hydrogels was taken out and soak in H_2O_2 solution (5 mM) for secondary crosslinking for 1 h. Subsequently, the hydrogels were transferred to deionized water at 40 °C for 10 min to remove uncross-linked polymers and H_2O_2 while inactivating the HRP enzyme. Finally, the hydrogels were freeze-dried and compressed to produce GH-NbBG. The GH and GH-BG hydrogels were prepared using the same method, except that NbBG was not added or replaced by BG. In addition, the same volume of BG microspheres tableting (BGT) was prepared using a pressure of 20 MPa.

The surface morphology and composition of the hydrogels were analyzed by SEM and FTIR. The compressive strength before and after swelling of GH-NbBG was tested by using cylindrical hydrogel (10 mm high × 8 mm diameter) and verified at room temperature on a universal mechanical tester (Shimadzu, Japan). The compression speed was set to 2 mm/min.

Self-swelling properties of GH-NbBG hydrogel: In order to simulate the characteristics of less blood supply at the bone augmentation position, the self-swelling property of hydrogels was tested by placing them on completely wet blotting paper. In addition, to simulate the mucosal pressure after implantation, a 5 g weight was placed on the hydrogels. The height of the hydrogels was measured using vernier callipers at 0, 24, 48 and 72 h.

2.4. In vitro angiogenesis evaluation

In order to prove that the ions dissolved from GH-NbBG play the function of angiogenesis, the extracts were used in *in vitro* experiment. Human umbilical vein endothelial cells (HUVECs) were used to investigate the *in vitro* angiogenesis by co-cultivating with Control, BG and NbBG extracts. Before detecting angiogenesis, the biocompatibility of GH-NbBG was first detected including cell attachment, proliferation and live/dead staining. Then, the tube formation assay, scratch assay and CD31 immunofluorescent staining were selected to evaluate angiogenesis. All the detailed including extracts preparation, cells culture and experimental procedure were provided in the supporting information.

2.5. In vitro osteogenic differentiation assessment and mechanism analysis

Mouse bone marrow mesenchymal stem cells (mBMSCs) were used to investigate the osteogenic differentiation of GH-NbBG. Similarly, the mBMSCs were cultured with Control, BG and NbBG extracts. The medium was replaced every 2–3 days. Alkaline phosphatase (ALP) activity was employed to investigate the osteogenic differentiation potential at day 7. The mBMSCs were fixed with 2.5% glutaraldehyde for 15 min and washed with PBS, and incubated in ALP stain working solution (Beyotime, China) for 30 min at room temperature. The reaction was stopped by removing the ALP stain working solution and rinsing with PBS. Stained cells were visualized with light microscope (Observer7, Zeiss, Germany).

The osteogenic differentiation mechanism analysis of GH-NbBG were researched by bioinformatic analysis and RNA sequencing (RNA-seq). In order to verify the correctness of mechanism speculation, the protein expressions of RUNX2 and OCN were analyzed by western bloting and immunofluorescent staining. The detailed experimental procedures were provided in supplementary data.

2.6. In vivo angiogenesis and bone augmentation evaluation

Surgical procedure and treatment: sprague-dawley rats (SD rats, male, 200–250 g) were purchased from the Laboratory Animal Center, Southern Medical University. All the animal procedures were performed following the protocol approved by the Institutional Animal Care (Guangdong Pharmaceutical University), and adequate measurements were taken to minimize pain and discomfort to the animals. The bone augmentation animal model was adapted from previous study [28]. After general anesthesia by intraperitoneal injection of pentobarbital (Nembutal, 3.5 mg/100 g), all the 28 rats were shaved the hair at head and disinfected with iodine. A sagittal incision of approximately 15 mm was made on the scalp, and the calvarium was exposed by blunt dissection. BGT, GH, GH-BG and GH-NbBG hydrogels with a diameter of 6 mm and thickness of 2 mm was inserted into subcutaneous, which was then closed with silk 3-0 suture. After feeding for 1 and 6 weeks, 4 rats of each group were sacrificed using an overdose of sodium pentobarbital. The rats killed at 1 week were perfused with Microfil (MV-112, Flow Tech, Inc., Carver, MA) after cardiac perfusion with heparinized saline and 4% paraformaldehyde solution. After keeping at 4 °C overnight, the hydrogels together with surrounding skull were cut off and the bone augmentation height was measured using vernier calipers.

Micro-CT analysis: After fixed in 10% of phosphate-buffered formalin for 5 days, the three-dimensional morphology was detected by Micro-CT (XTV160H, X-TEK Co., UK) with a voltage of 60 kV and an electric current of 67 mA. The voxel size after reconstruction was 25 × 25 × 25 μm. Based on the Micro-CT results, three-dimensional images were reconstructed by MIMICS (Materiaise's interactive medical image control system, Materialise Co., Belgium). The new bone volume at 6 weeks was determined using the analysis software.

Histological evaluation: Following Micro-CT scan, the samples were decalcified in 10% EDTA for 4 weeks and then embedded in paraffin

parallel to the sectioned surface. Serial cross-sections of decalcified samples were sectioned for hematoxylin and eosin (HE) and Masson's trichrome staining according to the manufacturer's instructions. In addition, the samples at 1 week were stained with immunohistochemistry of CD31 (1:200, Invitrogen) and VEGF (1:500, abcam), and the samples at 6 weeks were stained with OCN (1:200, Servicebio) and RUNX2 (1:500, Proteintech). Then images were captured by using CaseViewer (Hungary).

2.7. Statistical analysis

All the data were measured and expressed as the mean $\pm$ standard deviation (SD) for experiments conducted at least in triplicate. The statistical significances were determined *via* Student's *t*-test or one-way analysis. The difference was considered to be statistically significant when $P < 0.05$.

3. Results

3.1. Preparation and characteristics of GH-NbBG hydrogels

In this study, a double crosslinked bioactive GH-NbBG hydrogels were successfully prepared which was expected to be used for bone augmentation. The double crosslinking system including the schiff base reaction and enzymic catalytic reaction was shown in Fig. 1C. Specifically, GA-tyramine happened a schiff base reaction. Meanwhile, the oxidized hyaluronic acid (HA-CHO) underwent an enzymic catalytic reaction with the amino group of gelatin. The grafting of tyramine with the substitution degree of 0.103 mmol/g was tested by ^{1}H NMR as shown in Fig. S1. In addition to the typical peaks assigned to GA, the representative peaks ascribed to tyramine at 6.5–7.0 ppm were also observed in the spectrum of GA-tyramine, indicating that it was successfully modified to GA [29]. Moreover, the spectra of HA-CHO showed an extra chemical shift at approximately 4.8 ppm, which corresponded to –CHO [30]. To enhance the bioactivity of the hydrogel, NbBG microspheres were prepared and added to the GH-NbBG hydrogels. The EDS images showed that niobium was evenly distributed in the microspheres, and the doping of niobium did not change the physical and chemical properties (Fig. S2). Ion release behavior indicated that the Ca, Si and P ions release trend of NbBG was similar to BG. In addition, the Nb release was rising first and then decreasing, suggesting that Nb participated in the mineralization of NbBG (Fig. S3). The XPS results further confirmed that the peaks of Nb $3d_{5/2}$ and Nb $3d_{3/2}$ electrons were located at 207.6 eV and 210.3 eV for the NbBG, which confirms the Nb^{5+} oxidation state (Fig. S4). After addition into the hydrogel, both BG and NbBG were distributed uniformly in the double crosslinked network, while microspheres could not be seen in the GH group from SEM results (Fig. 2A). The FTIR results also showed that NbBG was successfully
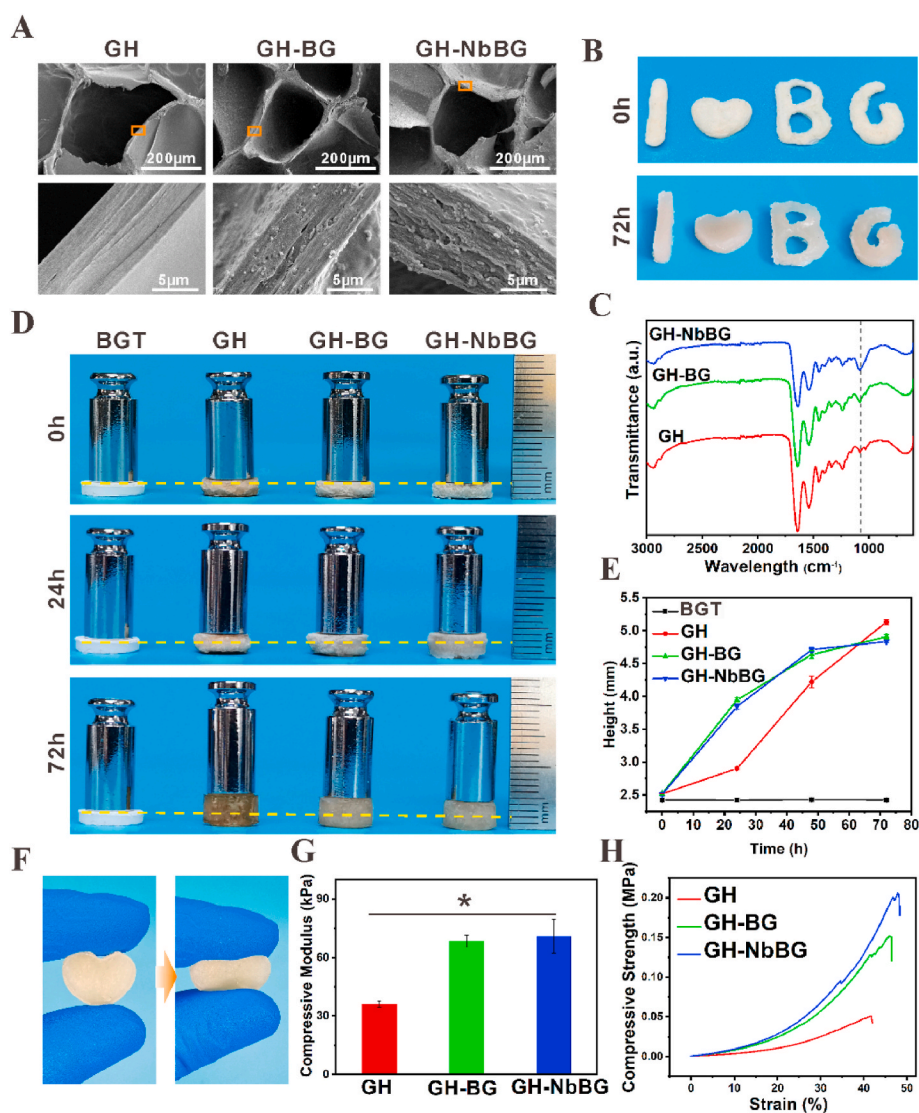

Fig. 2. Preparation and characterizations of GH, GH-BG and GH-NbBG hydrogels. (A) SEM images of GH, GH-BG and GH-NbBG at different magnification; (B) GH-NbBG hydrogels were individually prepared into the specific shapes of "*I love BG*"; (C) The FTIR spectra of GH, GH-BG and GH-NbBG hydrogels; (D) Self-swelling process of the hydrogels under 5 g load at 0, 24 and 72 h; (E) Quantitative analysis of the self-swelling process under 5 g loading; (F) Digital photo show the compressibility of GH-NbBG hydrogels; (G) Compressive modulus of the hydrogels; (H) Compressive stress-strain curve of the hydrogels. (*$P < 0.05$).

added in hydrogels with peaks at 1100 cm^{-1} representing the absorption peaks of Si–O–Si (Fig. 2C).

In clinical applications, bone augmentation scaffolds usually require personalized preparation because of the varying degree of alveolar ridge atrophy in different patients. Therefore, the GH-NbBG hydrogels were individually prepared into specific shapes of "*I love BG*", indicating their excellent plasticity that could be well adapted to the clinical applications (Fig. 2 B). To simulate the mucosal pressure after implantation, the self-swelling process was tested under 5 g loading (Fig. 2D). The swelling curve results showed that the height of hydrogels rises uniformly with increases nearly twice after 72 h, while BG tableting (BGT) did not change (Fig. 2E). Careful observation revealed that the swelling of GH was less than that of GH-BG and GH-NbBG at 24 h, which may be due to the interference of cross-linking after the BG and NbBG microspheres entered the hydrogels network (Fig. 2D and E). However, after 72 h, the height of GH-NbBG was 4.83 ± 0.02 mm, which was similar to GH (5.13 ± 0.04 mm).

In addition, mechanical properties and biodegradability of GH-NbBG hydrogels were also tested. The results showed that after the gelatin and hyaluronic acid degradation, BG and NbBG presented excellent mineralization properties at 5 days (Fig. S5A). The quality of the three groups of hydrogels decreased at 7 days of degradation. Subsequently, the degradation of GH accelerated, and the residual mass of GH was 41.02 ± 3.63% by 21 days. However, the remaining masses of GH-BG and GH-NbBG were 80.95 ± 3.37% and 80.22 ± 4.56% with no significant difference (Fig. S5B). Mechanical properties results indicated the hydrogels could withstand a certain amount of compression and completely return to its original shape by repeatedly pressing with fingers (Fig. 2F). Further quantitative detection found that the compressive modulus of GH-NbBG before and after swelling were 73.7 ± 13.7 KPa and 70.9 ± 8.6 KPa, which significantly enhanced in comparison with GH hydrogels ($P < 0.05$) (Fig. 2G, H and Fig. S6).

3.2. *In vitro angiogenesis of GH-NbBG hydrogels*

As a prerequisite of GH-NbBG to perform other functions, the biocompatibility was first detected as shown in Fig. S7. It is normal for GH hydrogels to promoting cell adhesion due to its similar composition to extracellular matrix. Moreover, the GH-BG and GH-NbBG hydrogels also promoted cell spreading, as a large number of pseudopods could be observed (Fig. S7A). The proliferation results showed that the cells proliferated slowly during the first few days. After 3 days, the cells proliferated rapidly in all 3 groups, and the GH-NbBG showed no significant difference compared with GH ($P > 0.05$) (Fig. S7B). The live/dead staining results also confirmed that almost no dead cells could be seen in the GH-NbBG group after culturing for 48 h (Fig. S7C). All these results indicated that GH-NbBG had excellent biocompatibility.

After material implantation, early angiogenesis is a key process for successful bone augmentation. Therefore, the *in vitro* angiogenesis properties of GH-NbBG hydrogels were further examined as shown in Fig. 3. In order to determine whether NbBG can promote angiogenesis, we excluded the interference of other hydrogel components and directly cultured HUVECs with BG and NbBG extracts (Table S1). The migration effect was studied via a scratch assay (Fig. 3D and E). The results showed that after 24 h of incubation, the remaining scratch width in the NbBG group was significantly smaller than that in the BG group based on the images and quantitative results, which indicated that NbBG significantly induced the migration of HUVECs. As the most direct evidence of angiogenesis, the tube formation effect of NbBG in matrigel was also investigated. As shown in Fig. 3A, the control group induced very limited tube formation, whereas extracts of BG and NbBG induced significantly more tube formation. In addition, quantitative analysis showed that the junction number and total length in the NbBG group were significantly more than that of the BG group (Fig. 3B and C). The CD31 immunostaining images also confirmed that the fluorescence intensity of NbBG were significantly stronger than that of the BG group (*P*
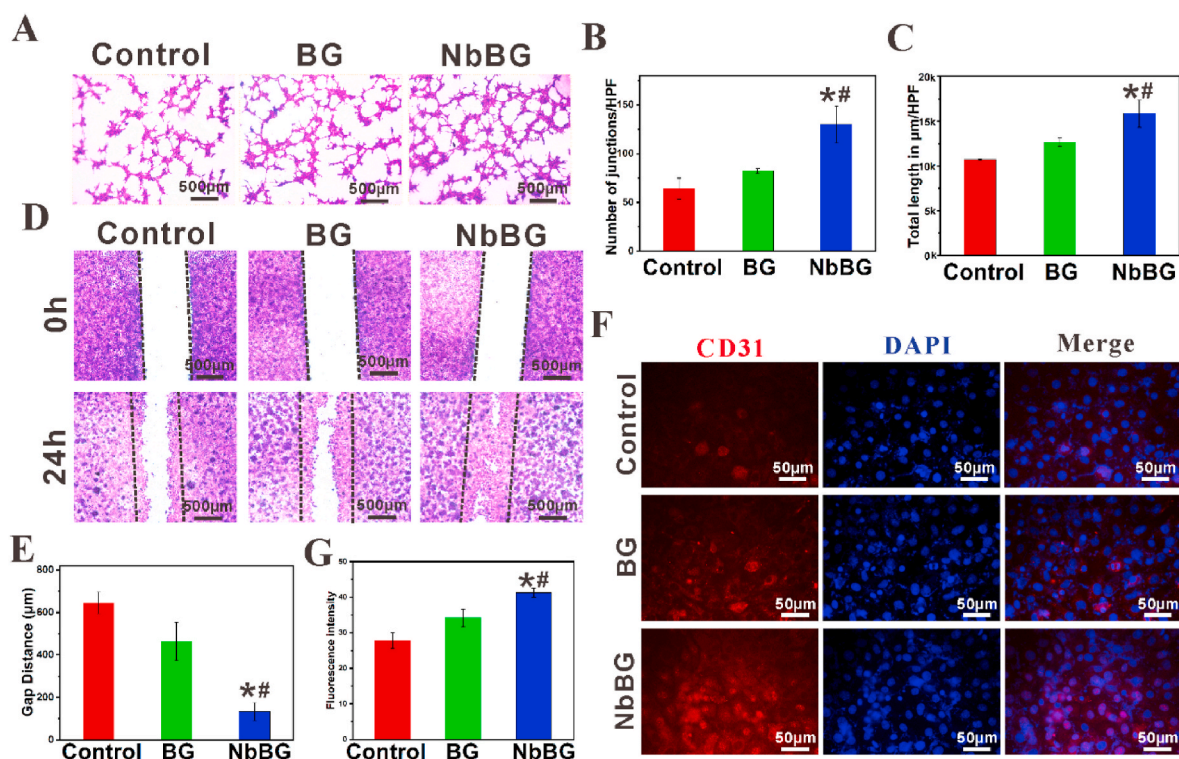

Fig. 3. *In vitro* angiogenesis of the hydrogels. (A) Tube formation of HUVECs stimulated by BG and NbBG for 12 h; (B) Quantitative analysis of junctions number; (C) Quantitative analysis of total length per high power field (HPF); (D) Representative images of scratch healing for migration cultured for 0 and 24 h staining with crystal violet; (E) Quantitative results of the remaining distance of scratch in each group by its fraction of initial defect at 0 h; (F) Immunostaining images of CD31 (red) and DAPI (blue); (G) Quantification of the immunostaining intensity of CD31. Notes: *$P < 0.05$ compared to Control; #$P < 0.05$ compared to BG.

< 0.05) (Fig. 3F and G). In summary, the GH-NbBG hydrogels had excellent biocompatibility and angiogenic properties.

3.3. Osteogenesis properties and mechanism of GH-NbBG promoting osteogenesis

The osteogenesis properties of the hydrogel were also studied. As an important reference for osteogenic differentiation, the ALP staining intensity of NbBG was significantly deepened compared with BG (Fig. 4A). Kyoto Encyclopedia of Genes and Genomes (KEGG) pathways enrichment analysis also confirmed that NbBG activated several osteogenic signaling pathways including the PI3K-Akt signaling pathway, MAPK signaling pathway, TGF-beta signaling pathway, Wnt signaling pathway (Fig. 4B). Moreover, the osteogenic differences between NbBG and BG were investigated in detail. Volcano plot result of differentially expressed genes showed that 28 genes were upregulated and 25 genes were down-regulated in NbBG group compared with BG (Fig. 4C). Although only a few genes were significantly different in expression, 10 genes were involved in bone formation including 5 osteogenesis related genes and 5 osteoclast related genes (Fig. 4D). More importantly, in comparison with BG, the NbBG simultaneously promoted osteogenic differentiation and downregulated the expression of osteoclast-related genes. All these results suggested that NbBG could significantly promote osteogenesis.

The mechanism of NbBG promoting osteogenesis was further studied. After careful analysis of the differentially expressed genes of BG and NbBG, we found that the Bglap and Bglap2 expression in NbBG were significantly up-regulated (Fig. 4D). Since Bglap and Bglap2 gene expression is regulated by transcription factors, we further examined RUNX2 expression of NbBG and found that it was significantly upregulated compared with the BG from western blotting results (Fig. 4F). Moreover, after transcription, Bglap will be translated into osteocalcin (OCN) which promotes bone formation. The OCN expression of NbBG

was further detected, and it was found that the protein expression was significantly up-regulated from both immunofluorescence staining (Fig. 4E, Fig. S9) and western blotting (Fig. 4F). Therefore, it can be reasonably speculated that NbBG promotes osteogenesis by activating RUNX2/Bglap signaling pathway (Fig. 4G).

3.4. In vivo synergetic angiogenesis and bone augmentation at the early stage of implantation

The *in vivo* synergetic processes of angiogenesis and bone augmentation caused by self-swelling at the early stage of implantation were studied by implanting BGT, GH, GH-BG and GH-NbBG hydrogels in a bone augmentation model for 7 days (Fig. 5A). The bone augmentation of GH-NbBG was achieved by self-swelling of the double crosslinked hydrogel. The height of GH-NbBG hydrogel had increased from 2 mm at the beginning of implantation to 4 mm after 7 days, based on measurements of skull samples (Fig. 5B, F), which was consistent with the self-swelling under weight bearing *in vitro* (Fig. 2D). However, the height of BGT was still 2 mm without any changes. In addition, the gross observation of tissue sections also confirmed that GH-NbBG hydrogels pushed away the surrounding soft tissue and the height of the hydrogels increased to 4 mm by self-swelling (Fig. 5C).

The *in vivo* angiogenic properties were also investigated. Since the greatest site of mucosal tension occurs in the central region of the bone augmentation, the central area was specifically observed (red dotted circle in Fig. 5D). Angiography results showed that the GH-NbBG hydrogels group had more blood vessels perfused by contrast agent than the GH-BG group (Fig. 5D). 3D reconstruction image was used to further observe the distribution of blood vessels by Micro-CT, as shown in Fig. 5E. In GH-NbBG group, a large number of blood vessels appeared in the central area of bone augmentation, while only a few vessels appeared in the GH-BG group. Longitudinal sections observation revealed that a large number of blood vessels also appeared inside the
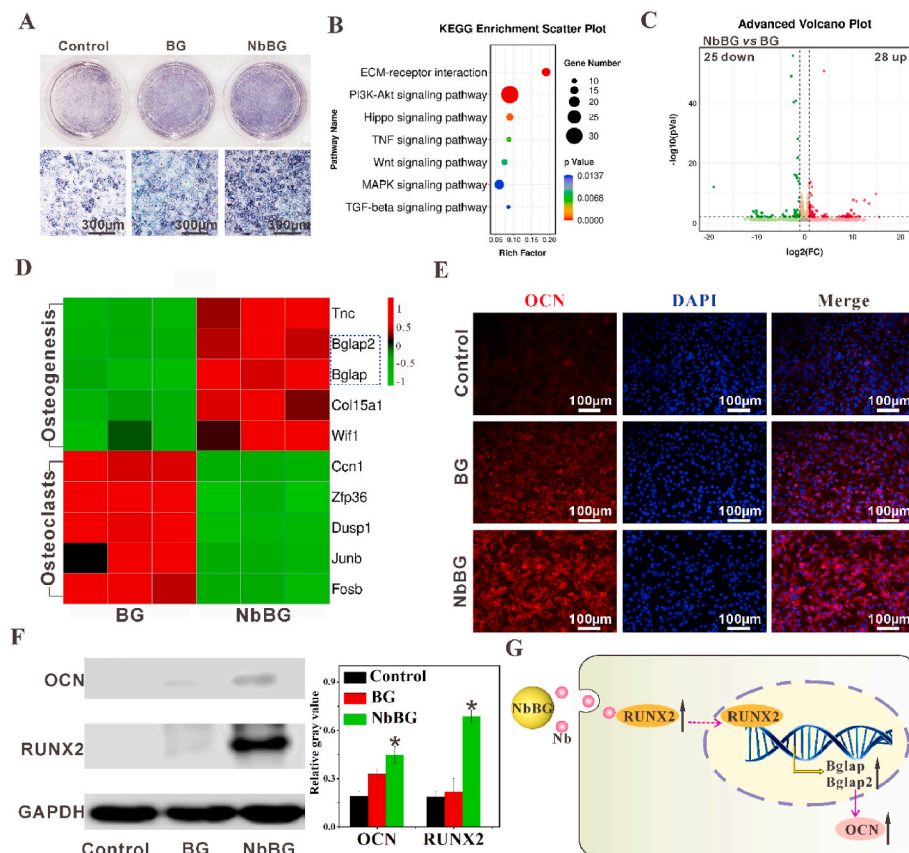

Fig. 4. Osteogenesis evaluation and mechanism of GH-NbBG hydrogel promoting osteogenesis. (A) ALP staining at 7 days; (B) The gene enrichment KEGG pathways analysis of NbBG *vs* Control; (C) Volcano plot of the differentially expressed genes between NbBG and BG groups. (≥2-fold difference, *P* value < 0.01; red: upregulated genes; green: downregulated genes); (D) Heat map of osteogenesis-related gene expression in NbBG compared to BG; (E) Immunofluorescence staining of OCN; (F) western bloting analysis of RUNX2 and OCN expression; (G) Schematic diagram of NbBG promoting osteogenesis mechanism. Notes: *P < 0.05 compared to BG.
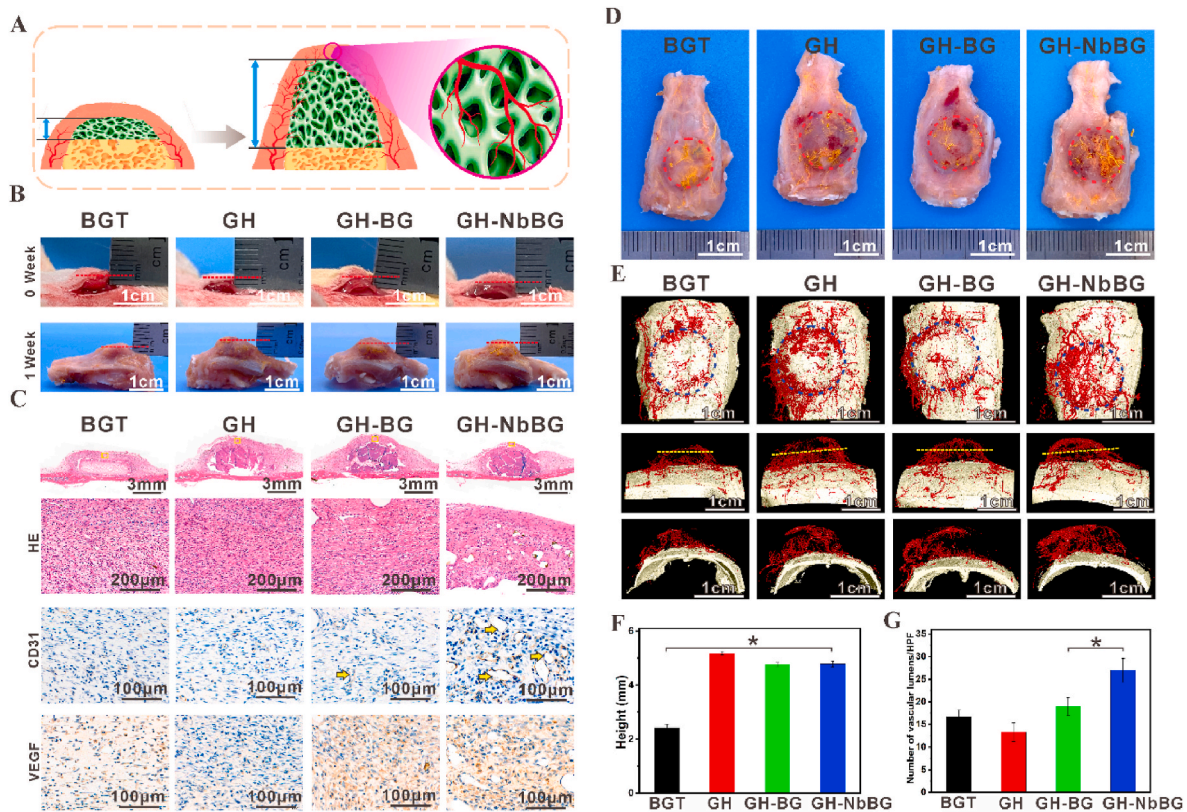
Fig. 5. *In vivo* synergetic angiogenesis and bone augmentation of GH-NbBG hydrogels at 7 days. (A) Schematic diagram of GH-NbBG hydrogels synergetic promotion angiogenesis and increase bone augmentation by self-swelling; (B) Measure the height of bone augmentation at the time of implantation and after 7 days; (C) Histological images of hydrogels with around tissues stained with HE, CD31 and VEGF (the first line was general view of longitudinal section, yellow arrows indicated blood vessels); (D) Gross observation of hydrogels together with surrounding tissue (red dotted circle indicates the central area of bone augmentation); (E) 3D reconstruction images of the hydrogels and surrounding tissue by Micro-CT analysis (blue dotted circle indicates the central area of bone augmentation); (F) Quantitative analysis of the height of bone augmentation; (G) Quantitative analysis of the vascular lumens number measured from the CD31 immunohistochemical images. (BGT was used as control group, *$P < 0.05$).

GH-NbBG hydrogels, suggesting that the hydrogels had been vascularized. Tissue sections were used to further observe the vascular microstructure at the top of the hydrogels (Fig. 5C). HE and Masson's trichrome staining results showed that a large number of vascular luminal structures were presented in the GH-NbBG hydrogels group (Fig. 5C, Fig. S10). CD31 immunohistochemical staining confirmed that these lumens were blood vessels with significantly deepened staining. Meanwhile, a large number of capillaries were observed, that could not be filled with contrast agent. Quantitative analysis showed that GH-NbBG hydrogels had more blood vessels than GH-BG group (Fig. 5G). In addition, a large number of VEGF positive proteins could be observed in the top area of GH-NbBG hydrogel (Fig. 5C). All these results suggested that the GH-NbBG hydrogels synergistically promoted angiogenesis and increased bone augmentation by self-swelling.

3.5. In vivo bone formation evaluation

In vivo new bone formation of GH, GH-BG and GH-NbBG hydrogels was studied at 6 weeks. All the hydrogels had closely attached to the skull surface without any space by observing the skull samples (Fig. 6A). However, the volume of the remaining hydrogels varies greatly. GH-BG and GH-NbBG still retained a large amount of organization, while GH group was almost completely degraded. In addition, careful observation showed that the remaining tissue of GH-NbBG was significantly larger than that of GH-BG (Fig. 6A). 3D reconstruction images of hydrogels also confirmed that the bone augmentation area of GH-NbBG was larger than that of GH-BG (Fig. 6B). In addition, some high-density shadows could be observed in both GH-NbBG and GH-BG groups from Micro-CT section

view, suggesting new bone formation. Further quantitative analysis showed that the new bone volume of GH-NbBG was larger than that of GH-BG ($P < 0.05$) (Fig. 6E). The morphology of the new bone was carefully observed in tissue sections (Fig. 6C, Fig. S11). Although the hydrogels had been tightly integrated with the skull according to the images of the skull, the hydrogel in the GH-BG group was still separated from the skull from the tissue section, and no mature lamellar bone could be observed. While the GH-NbBG group presented a large amount of immature new bone and lamellar bone. More importantly, the lamellar bone had been closely connected with the original skull. The final height of bone augmentation was also assessed. Although the hydrogels of GH-NbBG had been partially degraded, the final height was still greater than 2 mm. Quantitative analysis showed that the final bone increment height of GH-NbBG was 3.01 ± 0.14 mm which was greater than that of GH-BG ($P < 0.05$) (Fig. 6D). These results suggest that GH-NbBG promotes new bone formation in the late stage of implantation. Moreover, the mechanism of GH-NbBG promoting osteogenesis was verified (Fig. 6F). Immunohistochemical results showed that the OCN staining intensity of GH-NbBG was obviously enhanced in comparison with GH-BG, which was consistent with the results of *in vitro* experiments. However, the expression of RUNX2 was not obvious in either GH-BG or GH-NbBG groups. This phenomenon may be due to the RUNX2 expression had to be downregulated to form mature bone in the late stage of osteogenesis [31].

4. Discussion

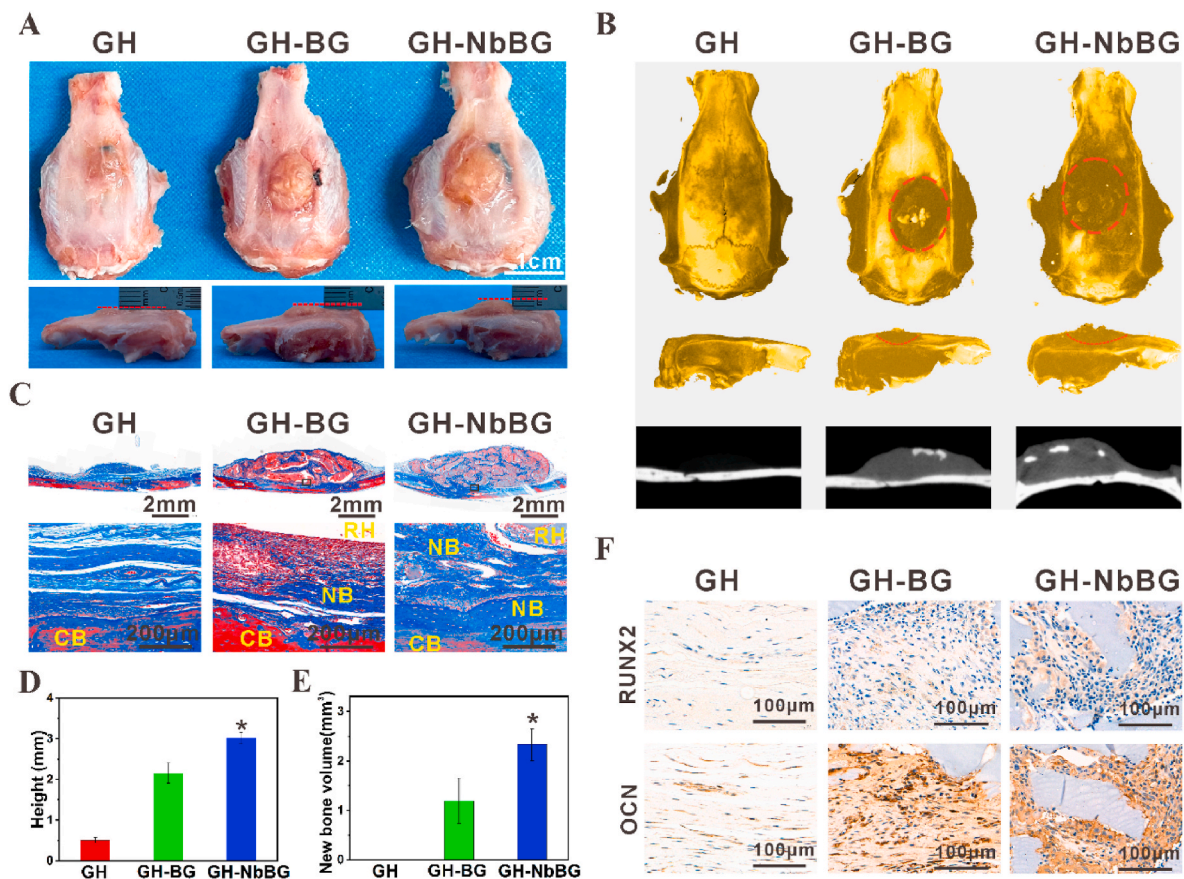In this study, inspired by the Chinese ancient myth of "*Pan Gu epoch*",

Fig. 6. *In vivo* new bone formation evaluation of GH, GH-BG and GH-NbBG hydrogels at 6 weeks. (A) General observation the bone augmentation position and the height of bone augmentation was measured laterally; (B) 3D reconstruction images of hydrogels and surrounding tissue by Micro-CT including top view, side view and section view; (C) Masson's trichrome staining images of the hydrogels with around tissues using different magnification (the second line was magnification of the black box in first column); (D) Quantitative analysis of the height of bone augmentation; (E) Quantitative analysis of new bone volume from Micro-CT; (F) Immunohistochemical staining of RUNX2 and OCN at the bone augmentation vertices. Symbols were residual hydrogels (RH), new bone (NB) and cortical bone (CB). * indicates a significant difference compared with the BG group, $P < 0.05$.

we successfully prepared the GH-NbBG hydrogels for bone augmentation by synergistic swelling and angiogenesis. We find a high degree of correspondence between myth and this research. In the myth of "*Pan Gu epoch*", the sky and earth were combined and inseparable at first, which corresponds to the amalgamation of the alveolar crest mucosa with cortical bone. Then, Pan Gu separated the sky from earth by stretching his body, which corresponds to the process that hydrogels are implanted submucosa to achieve bone augmentation through self-swelling. Finally, Pan Gu's body changed into mountains and rivers after his death, which corresponds to the hydrogel transforming into new bone and blood vessels after degradation, and achieving bone augmentation.

The atrophied alveolar ridge is the most important factor hindering the implementation of dental implants, which require extra bone augmentation [32]. Although many biomaterials have been attempted to achieve bone augmentation [33,34], the final bone augmentation heights are generally unsatisfactory. The main reason is that the materials will be degraded and compressed by mucosa during the period of osteogenesis, which reduces the height of bone augmentation [28]. In this experiment, the GH-NbBG hydrogels was successfully prepared for bone augmentation by taking advantage of self-swelling property after absorbing water. Finally, the height of the bone augmentation was nearly twice compared with the height of initial implantation. In fact, in other tissue repair applications, hydrogels are not expected to swelling including cartilage, skin and bone repair [35–37]. In other words, swelling is a disadvantage of hydrogels and many methods have been used to limit the swelling of hydrogels [6]. However, in the application of bone augmentation, we ingeniously turned this "disadvantage" of

hydrogel self-swelling into an advantage to achieve more new bone formation for dental implants. Considering that uncontrolled swelling will cause collapse, the double crosslinking method is used to control the volume of hydrogel including via the schiff base reaction and enzymic catalytic reaction. Previous studies have also reported that hydrogels are used for wound and osteochondral defect repair by constructing double crosslinking reactions to improve mechanical properties [9,38]. In this study, only one crosslinking ratio was adopted to increase the volume by two times, and further research is necessary to achieve precise control of the hydrogel volume by controlling the degree of crosslinking.

In addition to volume expansion, hydrogels must have excellent mechanical properties to resist mucosal pressure. In our design, NbBG microspheres are added to hydrogels, which effectively improves mechanical properties and avoids hydrogel cracking under compression. Previous studies also reported that inorganic substances in hydrogels improve the mechanical properties including tricalcium phosphate, hydroxyapatite, *etc*. [39,40]. The incorporation of inorganic components improves the regularity of the polymer hydrogel network structure, the degree of freedom of the crosslinked structure, and the flexibility of the polymer chain, thereby enhancing the mechanical strength of the hydrogels [11]. Different from previous reports, in our design the addition of NbBG significantly promoted material bioactivity, including osteogenesis and angiogenesis.

The early angiogenesis is the key point for bone augmentation after material implantation, as prolonged ischemia will cause material exposure [41]. Especially in the process of hydrogels expansion, the tension and ischemia of the surrounding mucosa will increase further.

Therefore, it is urgent to rapidly vascularize at the initial stage of implantation during the expansion process of hydrogel. Considering the only application of BG cannot meet the requirement of angiogenesis, NbBG was added to the hydrogels and achieved rapid angiogenesis. Similar reports also found that NbBG significantly stimulate the secretion of VEGF, which is similar to the findings of this study [42]. Therefore, the GH-NbBG hydrogels successfully combined self-swelling and vascularization to achieve a 2-fold increase in bone augmentation.

After the early angiogenesis of the material implantation, the later rapid osteogenesis will help to shorten the treatment course. In our research, the addition of niobium significantly promoted the osteogenesis process. Previous studies have also found that niobium can promote the repair of bone defects both *in vivo* and *in vitro* experiments [26]. However, the mechanism by which niobium promotes osteogenesis remains unclear. In this experiment, we first observed the up-regulation expression of Bglap and Bglap2 by bioinformatic analysis. It has been confirmed that OCN is encoded by Bglap and Bglap2 in mice [43,44]. The OCN is specifically expressed in osteoblasts which has been accepted as a reliable marker for predicting osteogenic progress in bone tissue engineering [45]. In this study, we observed an upregulation of OCN, suggesting that NbBG promotes osteogenesis by activating OCN. In addition, the gene expression of Bglap and Bglap2 is regulated by transcription factors. Considering that RUNX2 is the first transcription factor required for determination of the osteoblast lineage [46], we further observed that the expression of RUNX2 was up-regulated after culturing for 7 days. Previous studies have confirmed that RUNX2 triggers the expression of major bone matrix genes during the early stages of osteoblast differentiation including Bglap2 [31]. However, although RUNX2 promotes osteogenic differentiation in the early stage of osteogenesis, it will inhibit osteoblast differentiation into osteocytes [47]. Therefore, the RUNX2 expression will be downregulated at the late stage of osteogenesis [48], which is consistent with our observation that the RUNX2 expression is not significant after 6 weeks of implantation. In summary, we speculate that NbBG promotes osteogenesis through activation RUNX2/Bglap pathways. However, the mechanism by which NbBG activates RUNX2 remains unclear, and further research is necessary to explore the upstream signal pathways of RUNX2 activated by NbBG.

5. Conclusion

In this study, a NbBG added double-crosslinked GH-NbBG hydrogel was successfully prepared. Inspired by the myth of "*Pan Gu epoch*", the hydrogel achieved a two-fold increase in height by utilizing self-swelling properties, which ingeniously changed the "disadvantage" of self-swelling into an advantage. Meanwhile, the GH-NbBG significantly promoted angiogenesis at the early stage of implantation. In addition, the hydrogels promoted osteogenesis by activating RUNX2/Bglap signaling pathway. Therefore, the GH-NbBG hydrogels have great potential for clinical application in bone augmentation, and this study provided novel ideas for the application of hydrogels by using the self-swelling "disadvantage" properties.

Ethics approval and consent to participate

The study was approved by the ethics committee (Full name: GuangDong Pharmaceutical University Experimental Animal Ethics Committee Inspection) (Reference number: gdpulac2021179), GuangDong Pharmaceutical University, China.

CRediT authorship contribution statement

Fujian Zhao: Methodology, Writing – original draft, preparation, Formal analysis, Data curation. **Zhen Yang:** Methodology, Writing – original draft, preparation, Investigation, Formal analysis. **Huacui Xiong:** Formal analysis, Data curation. **Yang Yan:** Software, Visualization. **Xiaofeng Chen:** Project administration, Writing-review. **Longquan Shao:** Supervision, Project administration.

Declaration of competing interest

The authors declared that they have no conflicts of interest to this work.

Appendix A. Supplementary data

Supplementary data to this article can be found online at https://doi.org/10.1016/j.bioactmat.2022.09.007.

References

[1] L. Sanchez-Labrador, P. Molinero-Mourelle, F. Perez-Gonzalez, L.M. Saez-Alcaide, J.C.-B. Brinkmann, J.L.-Q. Martinez, J.M. Martinez-Gonzalez, Clinical performance of alveolar ridge augmentation with xenogeneic bone block grafts versus autogenous bone block grafts. A systematic review, J. Stomatol. Oral Maxi. 122 (3) (2021) 293–302.

[2] Y. Xie, S. Li, T. Zhang, C. Wang, X. Cai, Titanium mesh for bone augmentation in oral implantology: current application and progress, Int. J. Oral Sci. 12 (1) (2020) 37.

[3] J. Garner, D. Davidson, G.J. Eckert, C.T. Barco, H. Park, K. Park, Reshapable polymeric hydrogel for controlled soft-tissue expansion: in vitro and in vivo evaluation, J. Contr. Release 262 (2017) 201–211.

[4] K. Elkhoury, C.S. Russell, L. Sanchez-Gonzalez, A. Mostafavi, T.J. Williams, C. Kahn, N.A. Peppas, E. Arab-Tehrany, A. Tamayol, Soft-nanoparticle functionalization of natural hydrogels for tissue engineering applications, Adv. Healthcare Mater. 8 (18) (2019), 1900506.

[5] X. Xue, Y. Hu, Y. Deng, J. Su, Recent advances in design of functional biocompatible hydrogels for bone tissue engineering, Adv. Funct. Mater. 31 (19) (2021), 2009432.

[6] Y.W. Zhan, W.J. Fu, Y.C. Xing, X.M. Ma, C.Y. Chen, Advances in versatile anti-swelling polymer hydrogels, Mater. Sci. Eng. C Mater. Biol. Appl. 127 (2021), 112208.

[7] T. Chen, Y. Wang, J. Xie, X. Qu, C. Liu, Lysozyme amyloid fibril-integrated PEG injectable hydrogel adhesive with improved antiswelling and antibacterial capabilities, Biomacromolecules 23 (3) (2022) 1376–1391.

[8] C. Wang, Y. Luo, X. Cao, B. Li, Z. Luo, Supramolecular polyurea hydrogels with anti-swelling capacity, reversible thermochromic properties, and tunable water content and mechanical performance, Polymer 233 (2021), 124213.

[9] X. Zhu, T.T. Chen, B. Feng, J. Weng, K. Duan, J. Wang, X. Lu, Biomimetic bacterial cellulose-enhanced double-network hydrogel with excellent mechanical properties applied for the osteochondral defect repair, ACS Biomater. Sci. Eng. 4 (10) (2018) 3534–3544.

[10] W. Liu, W. Bi, Y. Sun, L. Wang, X. Yu, R. Cheng, Y. Yu, W. Cui, Biomimetic organic-inorganic hybrid hydrogel electrospinning periosteum for accelerating bone regeneration, Mater. Sci. Eng. C Mater. Biol. Appl. 110 (2020), 110670.

[11] Y.Y. Chu, X.F. Song, H.X. Zhao, Water-swellable, tough, and stretchable inorganic-organic sulfoaluminate cement/polyacrylamide double-network hydrogel composites, J. Appl. Polym. Sci. 136 (35) (2019), 47905.

[12] Y. Chen, W. Sheng, J. Lin, C. Fang, J. Deng, P. Zhang, M. Zhou, P. Liu, J. Weng, F. Yu, D. Wang, B. Kang, H. Zeng, Magnesium oxide nanoparticle coordinated phosphate-functionalized chitosan injectable hydrogel for osteogenesis and angiogenesis in bone regeneration, ACS Appl. Mater. Interfaces 14 (6) (2022) 7592–7608.

[13] Z. Yang, F. Zhao, W. Zhang, Z. Yang, M. Luo, L. Liu, X. Cao, D. Chen, X. Chen, Degradable photothermal bioactive glass composite hydrogel for the sequential treatment of tumor-related bone defects: from anti-tumor to repairing bone defects, Chem. Eng. J. 419 (2021), 129520.

[14] S. Gupta, S. Majumdar, S. Krishnamurthy, Bioactive glass: a multifunctional delivery system, J. Contr. Release 335 (2021) 481–497.

[15] H.O. Simila, A.R. Boccaccini, Sol-gel bioactive glass containing biomaterials for restorative dentistry: a review, Dent. Mater. 38 (5) (2022) 725–747.

[16] V. Lalzawmliana, A. Anand, M. Roy, B. Kundu, S.K. Nandi, Mesoporous bioactive glasses for bone healing and biomolecules delivery, Mater. Sci. Eng. C Mater. Biol. Appl. 106 (2020), 110180.

[17] F. Zhao, B. Lei, X. Li, Y. Mo, R. Wang, D. Chen, X. Chen, Promoting in vivo early angiogenesis with sub-micrometer strontium-contained bioactive microspheres through modulating macrophage phenotypes, Biomaterials 178 (2018) 36–47.

[18] D.H.J. Jager, F. Maarse, T. Klausch, K.H. Karagozoglu, C.M. ten Bruggenkate, G. K. Sandor, J. Wolff, E.A.J.M. Schulten, Wound dehiscences following pre-implant

bone augmentation with autogenous iliac crest bone grafts: a retrospective cohorts study, Int. J. Oral Implant. 12 (2) (2019) 227–236.

[19] X. He, Y. Liu, Y. Tan, L.M. Grover, J. Song, S. Duan, D. Zhao, X. Tan, Rubidium-containing mesoporous bioactive glass scaffolds support angiogenesis, osteogenesis and antibacterial activity, Mater Sci Eng C Mater Biol Appl 105 (2019), 110155.

[20] E.J. Ryan, A.J. Ryan, A. Gonzalez-Vazquez, A. Philippart, F.E. Ciraldo, C. Hobbs, V. Nicolosi, A.R. Boccaccini, C.J. Kearney, F.J. O'Brien, Collagen scaffolds functionalised with copper-eluting bioactive glass reduce infection and enhance osteogenesis and angiogenesis both in vitro and in vivo, Biomaterials 197 (2019) 405–416.

[21] S. Kargozar, F. Baino, S. Hamzehlou, R.G. Hill, M. Mozafari, Bioactive glasses: sprouting angiogenesis in tissue engineering, Trends Biotechnol. 36 (4) (2018) 430–444.

[22] V.M. Schatkoski, T.L.d.A. Montanheiro, B.R. Canuto de Menezes, R.M. Pereira, K. F. Rodrigues, R.G. Ribas, D.M. da Silva, G.P. Thim, Current advances concerning the most cited metal ions doped bioceramics and silicate-based bioactive glasses for bone tissue engineering, Ceram. Int. 47 (3) (2021) 2999–3012.

[23] N. Gupta, D. Santhiya, S. Murugavel, A. Kumar, A. Aditya, M. Ganguli, S. Gupta, Effects of transition metal ion dopants (Ag, Cu and Fe) on the structural, mechanical and antibacterial properties of bioactive glass, Colloid. Surface. 538 (2018) 393–403.

[24] L. de Siqueira, T.M.B. Campos, S.E.A. Camargo, G.P. Thim, E.S. Triches, Structural, crystallization and cytocompatibility evaluation of the 45S5 bioglass-derived glass-ceramic containing niobium, J. Non-Cryst. Solids 555 (2021) 120629.

[25] G.d.S. Balbinot, V.C. Branco Leitune, D. Ponzoni, F.M. Collares, Bone healing with niobium-containing bioactive glass composition in rat femur model: a micro-CT study, Dent. Mater. 35 (10) (2019) 1490–1497.

[26] U.P.L. de Souza, J.H. Lopes, F.V. Ferreira, R.A. Martin, C.A. Bertran, J.A. Camilli, Evaluation of effectiveness of 45S5 bioglass doped with niobium for repairing critical-sized bone defect in in vitro and in vivo models, J. Biomed. Mater. Res., Part A 108 (3) (2020) 446–457.

[27] G.d.S. Balbinot, E.A.d.C. Bahlis, F. Visioli, V.C.B. Leitune, R.M.D. Soares, F. M. Collares, Polybutylene-adipate-terephthalate and niobium-containing bioactive glasses composites: development of barrier membranes with adjusted properties for guided bone regeneration, Mater. Sci. Eng. C Mater. Biol. Appl. 125 (2021), 112115.

[28] L.A. Kinard, R.L. Dahlin, J. Lam, S. Lu, E.J. Lee, F.K. Kasper, A.G. Mikos, Synthetic biodegradable hydrogel delivery of demineralized bone matrix for bone augmentation in a rat model, Acta Biomater. 10 (11) (2014) 4574–4582.

[29] K. Ren, C. He, Y. Cheng, G. Li, X. Chen, Injectable enzymatically crosslinked hydrogels based on a poly(L-glutamic acid) graft copolymer, Polym. Chem. 5 (17) (2014) 5069–5076.

[30] S. Liu, X. Liu, Y. Ren, P. Wang, Y. Pu, R. Yang, X. Wang, X. Tan, Z. Ye, V. Maurizot, B. Chi, Mussel-inspired dual-cross-linking hyaluronic acid/ε-polylysine hydrogel with self-healing and antibacterial properties for wound healing, ACS Appl. Mater. Interfaces 12 (25) (2020) 27876–27888.

[31] T. Komori, Regulation of bone development and extracellular matrix protein genes by RUNX2, Cell Tissue, Res. 339 (1) (2010) 189–195.

[32] A. Aloy-Prosper, E. Carramolino-Cuellar, D. Penarrocha-Oltra, D. Soto-Penaloza, M. Penarrocha-Diago, Intraoral onlay block bone grafts versus cortical tenting technique on alveolar ridge augmentations: a systematic review, Med. Oral, Patol. Oral Cirugía Bucal 27 (2) (2022) E181–E190.

[33] X. Liu, Y. Miao, H. Liang, J. Diao, L. Hao, Z. Shi, N. Zhao, Y. Wang, 3D-printed bioactive ceramic scaffolds with biomimetic micro/nano-HAp surfaces mediated cell fate and promoted bone augmentation of the bone-implant interface in vivo, Bioact. Mater. 12 (2022) 120–132.

[34] E. Shamsoddin, B. Houshmand, M. Golabgiran, Biomaterial selection for bone augmentation in implant dentistry: a systematic review, "J. Adv. Pharm. Technol. Research"" (JAPTR)" 10 (2) (2019) 46–50.

[35] J.J. Xu, R.N. Jin, X.Y. Ren, G.H. Gao, Cartilage-inspired hydrogel strain sensors with ultrahigh toughness, good self-recovery and stable anti-swelling properties, J. Mater. Chem. 7 (44) (2019) 25441–25448.

[36] X. Du, Y. Hou, L. Wu, S. Li, A. Yu, D. Kong, L. Wang, G. Niu, An anti-infective hydrogel adhesive with non-swelling and robust mechanical properties for sutureless wound closure, J. Mater. Chem. B 8 (26) (2020) 5682–5693.

[37] J. Choi, J. Lee, M.E. Shin, S. Been, D.H. Lee, G. Khang, Eggshell membrane/gellan gum composite hydrogels with increased degradability, biocompatibility, and anti-swelling properties for effective regeneration of retinal pigment epithelium, Polymers 12 (12) (2020) 2941.

[38] L. Wang, X. Zhang, K. Yang, Y.V. Fu, T. Xu, S. Li, D. Zhang, L.-N. Wang, C.-S. Lee, A novel double-crosslinking-double-network design for injectable hydrogels with enhanced tissue adhesion and antibacterial capability for wound treatment, Adv. Funct. Mater. 30 (1) (2020), 1904156.

[39] Z. Li, W. Mi, H. Wang, Y. Su, C. He, Nano-hydroxyapatite/polyacrylamide composite hydrogels with high mechanical strengths and cell adhesion properties, Colloids Surf., B 123 (2014) 959–964.

[40] Y. Zhang, Z. Li, Z. Wang, B. Yan, A. Shi, J. Xu, J. Guan, L. Zhang, P. Zhou, Y. Mao, Mechanically enhanced composite hydrogel scaffold for in situ bone repairs, Mater. Sci. Eng. C Mater. Biol. Appl. 134 (2022) 112700.

[41] V. Chopra, J. Thomas, A. Sharma, V. Panwar, S. Kaushik, S. Sharma, K. Porwal, C. Kulkarni, S. Rajput, H. Singh, K. Jagavelu, N. Chattopadhyay, D. Ghosh, Synthesis and evaluation of a zinc eluting rGO/hydroxyapatite nanocomposite optimized for bone augmentation, ACS Biomater. Sci. Eng. 6 (12) (2020) 6710–6725.

[42] V. Miguez-Pacheco, D. de Ligny, J. Schmidt, R. Detsch, A.R. Boccaccini, Development and characterization of niobium-releasing silicate bioactive glasses for tissue engineering applications, J. Eur. Ceram. Soc. 38 (3) (2018) 871–876.

[43] C.R. Diegel, S. Hann, U.M. Ayturk, J.C.W. Hu, K.-E. Lim, C.J. Droscha, Z.B. Madaj, G.E. Foxa, I. Izaguirre, N. Paracha, B. Pidhaynyy, T.L. Dowd, A.G. Robling, M. L. Warman, B.O. Williams, V.A.I.V.T. Core, An osteocalcin-deficient mouse strain without endocrine abnormalities, PLoS Genet. 16 (5) (2020), e1008361.

[44] T. Komori, What is the function of osteocalcin? J. Oral Biosci. 62 (3) (2020) 223–227.

[45] J.-H. Hyung, C.-B. Ahn, C.-J. Je, Blue mussel (Mytilus edulis) protein hydrolysate promotes mouse mesenchymal stem cell differentiation into osteoblasts through upregulation of bone morphogenetic protein, Food Chem. 242 (2018) 156–161.

[46] T. Komori, Regulation of proliferation, differentiation and functions of osteoblasts by Runx2, Int. J. Mol. Sci. 20 (7) (2019) 1694.

[47] K. Gomathi, N. Akshaya, N. Srinaath, A. Moorthi, N. Selvamurugan, Regulation of Runx2 by post-translational modifications in osteoblast differentiation, Life Sci. 245 (2020), 117389.

[48] S. Vimalraj, B. Arumugam, P.J. Miranda, N. Selvamurugan, Runx2: structure, function, and phosphorylation in osteoblast differentiation, Int. J. Biol. Macromol. 78 (2015) 202–208.